Geochemical Perspectives Letters

Dust transport enhanced land surface weatherability in a cooling world

Y. Yang[1*], A. Galy[2], J. Zhang[3*], F. Lambert[4], M. Zhang[3], F. Zhang[5], X. Fang[1,6]

https://doi.org/10.7185/geochemlet.2322

Abstract

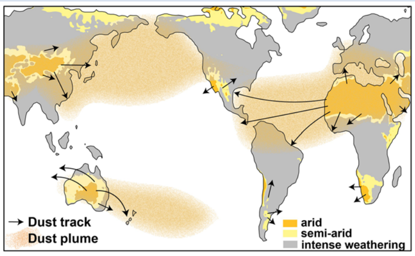

The weatherability of exposed silicate rocks drives the efficiency of climatic feedback on the geological carbon cycle through silicate weathering. However, the controls and evolution of land surface weatherability are not fully understood. Tectonically induced exposure of fresh silicates can induce a wide range of weatherability, depending on the maturity and lithology of the exhumed rocks. Here, we propose that aeolian dust has potentially been pivotal in sustaining land surface weatherability during global cooling. Our analysis of palaeoclimate simulations shows an additional transport of 1072 ± 69 Tg yr^{-1} of dust to regions with precipitation of more than 400 mm yr^{-1} during the Last Glacial Maximum compared to the pre-industrial period. As dust mainly contains fresh minerals with high surface areas, such dust transport markedly increases land surface weatherability, yielding an additional atmospheric CO_2 consumption of 0.431 ± 0.030 Tmol yr^{-1}, which would offset the reduced silicate weathering induced by weaker climatic forcing. It is suggested that a dustier world could increase global land surface weatherability, leading to a more buffered carbon cycle that sustained low atmospheric CO_2 levels.

Received 7 February 2023 | Accepted 12 June 2023 | Published 6 July 2023

Introduction

Land surface weatherability is the susceptibility of the land surface to chemical weathering (*e.g.*, Kump and Arthur, 1997). Silicate weathering is a key negative feedback that regulates the long term global carbon cycle (*e.g.*, Walker *et al.*, 1981). Therefore, together with the amount of silicate rocks in the critical zone, the weatherability of those silicate rocks has acted as an important variable in silicate weathering and the associated atmospheric carbon dioxide consumption. Variation in land surface weatherability was proposed as the dominant mechanism regulating the long term evolution of atmospheric carbon dioxide levels in the Phanerozoic (*e.g.*, Francois and Walker, 1992; Kump and Arthur, 1997; Caves *et al.*, 2016; Caves Rugenstein *et al.*, 2019). In particular, inverse modelling of marine proxies suggested that the Neogene cooling was driven by a rise in weatherability over time (Caves Rugenstein *et al.*, 2019), which may have been caused by the uplift of the Himalaya-Tibetan Plateau (*e.g.*, Raymo *et al.*, 1988; Kump and Arthur, 1997) and in combination with the exposure of Mg-rich lithologies in East and Southeast Asia (Park *et al.*, 2020; Yang *et al.*, 2021). Nevertheless, all of these studies suggest the dominant control of denudation of the continents on silicate weatherability. However, the temporal evolution of denudation fluxes during the late Cenozoic on the Himalaya-Tibetan Plateau and globe remains controversial (*e.g.*, Métivier *et al.*, 1999; Clift, 2006; Herman *et al.*, 2013; Lenard *et al.*, 2020).

Reconstructing land surface weatherability is not easy because it has always been affected by different factors, *e.g.*, tectonic activity, mountain building, surface lithology, glacier erosion, and vegetation cover (Francois and Walker, 1992). Unlike those proposed influencing factors of weatherability, here we propose that aeolian dust plays a role in sustaining high land surface weatherability in a cooling world. Aeolian dust is transported from arid sources to less arid areas, which can increase global land surface weatherability in two ways. First, the transport of less altered fine grained material to a more humid environment leads to a net increase in land surface weatherability. Second, aeolian dust provides nutrients to the vegetation (Ridgwell, 2002), which further increases silicate weathering rates. To test this idea, here we quantify the increase in dust deposition fluxes to the less arid continental regions and the associated atmospheric CO_2 consumption caused by silicate weathering between the preindustrial (PI) period and the Last

1. State Key Laboratory of Tibetan Plateau Earth System Science, Environment and Resources (TPESER), Institute of Tibetan Plateau Research, Chinese Academy of Sciences, Beijing 100101, China
2. Centre de Recherches Pétrographiques et Géochimiques, UMR7358, CNRS - Université de Lorraine, Nancy 54500, France
3. Department of Atmospheric and Oceanic Sciences, School of Physics, Peking University, Beijing 100871, China
4. Institute of Geography, Pontifical Catholic University of Chile, Chile
5. State Key Laboratory of Loess and Quaternary Geology, Institute of Earth Environment, Chinese Academy of Sciences, Xi'an 710075, China
6. University of Chinese Academy of Sciences, Beijing 100049, China
* Corresponding authors (emails: yangyibo@itpcas.ac.cn; jzhangcn@pku.edu.cn).

Glacial Maximum (LGM), because global dust cycles in the two periods are only well constrained by palaeo-dust record and climate modelling.

Results and Discussion

We conducted palaeoclimate simulations in our study (Figs. S-1 to S-3), where the preindustrial experiment (called PI-Exp) represents the warm condition of the last few kyr, and the LGM experiment (called LGM-Exp) corresponds to the cold condition ~21 kyr ago. To reveal the uncertainty of modelling data, we also collected another four modelling results from previous studies (Supplementary Information). The mean dust deposition flux over land and standard error of all five data sets are illustrated in Figure 1. We also summed the PI and LGM dust deposition fluxes from each model based on the mean annual precipitation (MAP) ranges (Fig. S-4). All the modelling results showed enhanced LGM dust deposition in terms of flux and spatial extent compared to PI conditions (Figs. 1, S-4). Dust deposition is high in the arid region around deserts in Central and East Asia, North Africa and Australia. However, the simulations clearly show that dust has also been transported to regions where the climate is wetter (Figs. S-1 to S-4). For both PI and LGM simulations, the amount of dust transported to regions with MAP >400 mm and >200 mm accounts for ~31 % and ~47 % of the global dust deposition flux in both simulations, respectively, despite the expansion of the arid regions during the LGM. Global land dust deposition has increased in almost all MAP zones during the LGM (Fig. 2a). The global net increases in aeolian dust (LGM-Exp minus PI-Exp) are 1621 ± 99 Tg yr^{-1} and 1072 ± 69 Tg yr^{-1} for regions with MAP >200 mm and >400 mm, respectively.

Dust promotes weatherability. The intensity of dust silicate weathering is strongly dependent on climatic conditions (*e.g.*, Goddéris *et al.*, 2010, 2013). In arid regions, the scarcity of precipitation and vegetation limits the weathering of silicate minerals, as seen by a low degree of Na depletion in silicates (Fig. S-5). In particular, a silicate Na_2O/Al_2O_3 ratio of 0.17 in arid regions with MAP <200 mm is slightly less than, but close to, that of 0.20 for unweathered upper continental crust (Figs. S-5, S-6). However, when the dust settles in more humid zones, silicates will be more prone to weathering, as seen by the much lower Na_2O/Al_2O_3 ratio (Fig. S-7a). Such dust has even become the main provider of fresh silicates and nutrients to the biosphere in some extreme scenarios where the local supply of fresh rocks is insufficient. For example, on the Hawaiian basaltic bedrock, much of the soil inorganic element originates from China and central Asian deserts (*e.g.*, Kurtz *et al.*, 2001). In addition, the fining of dust during long distance transport produces material with a greater surface area that promotes weathering.

Dust exerts important biogeochemical controls on the downwind terrestrial ecosystems of humid regions (Ridgwell, 2002) because 1) its mineralogy and grain size strongly influence the water- and nutrient-holding properties of the soil, and 2) it is a source of nutrients for some ecosystems. For example, in Amazonia, the soils are already highly weathered and nutrient-depleted, and dust transported across the Atlantic supports the ecosystems (Swap *et al.*, 1992). Some soils on the Hawaiian Islands suggest an analogous situation (Chadwick *et al.*, 1999). Therefore, *via* the fertilisation of vegetation, dust settling in areas with such highly weathered soils facilitates the silicate weathering process.

Weathering of aeolian dust is also pronounced in broad, less humid regions. Rainfall composition provides a valuable approach for addressing dust weathering kinetics. Rainfall compositions in less humid North China show high $^{87}Sr/^{86}Sr$ and low Ca/Sr ratios (Rao *et al.*, 2017), corresponding to fast dissolution of some silicates. Dust silicate weathering can also be found in Himalayas with heavy monsoon rainfall. The precipitation composition in Bangladesh and Nepal (Galy and France-Lanord, 1999) can be well explained by the mixing of silicate with low Ca/Sr ratios and Himalayan carbonate and sea salts with high Ca/Sr ratios. This evidence suggests that part of the dust is rapidly weathered in the atmosphere or shortly after deposition, increasing the weatherability.

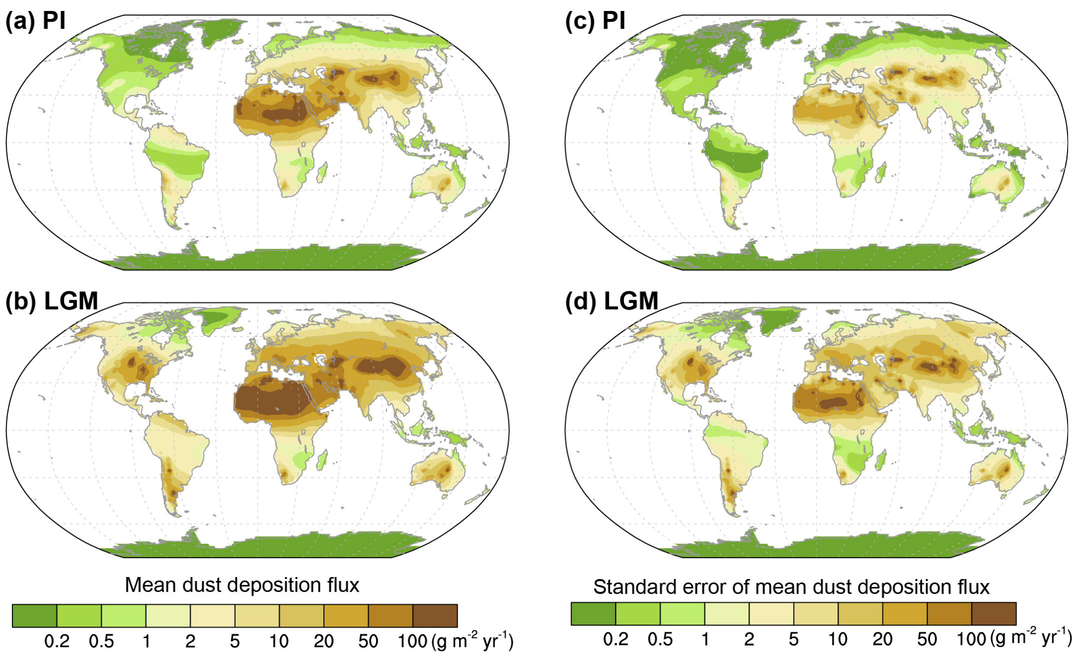

Figure 1 Mean land dust deposition fluxes **(a, b)** and their standard error **(c, d)** in experiments of preindustrial (PI) and Last Glacial Maximum (LGM) periods integrated from five climate model results (see Methods).

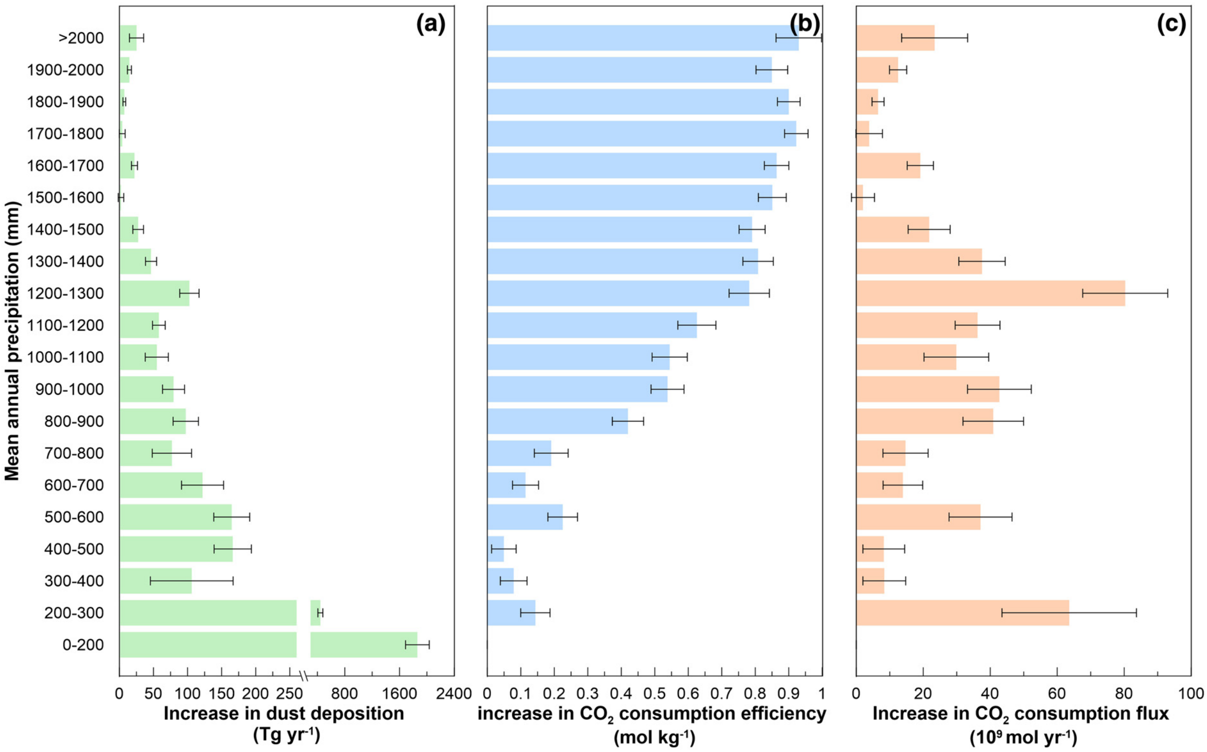

Figure 2 Increases in land dust deposition **(a)**, efficiency **(b)** and flux **(c)** of atmospheric CO_2 consumption by silicate weathering in the LGM compared with the PI categorised by mean annual precipitation (MAP). Note that increases in CO_2 consumption efficiency (a measure of the amount of CO_2 consumed by silicate weathering *per* kilogram rock) and flux in each zone with MAP >200 mm are estimated from the differences in CO_2 consumption efficiency and flux between those zones and the arid region (MAP <200 mm). Error bars show one standard error of the mean.

In addition, dust weathering involves not only silicates but also carbonates (Goddéris *et al.*, 2010). Due to abundant carbonate in dust and its rapid weathering rates in Mississippi loess, dolomite weathering can contribute to as high as 90 % CO_2 consumption of overall dust weathering (Goddéris *et al.*, 2010, 2013). Carbonate weathering can consume CO_2 on time scales shorter than a million years, and dust transport thus enhances the overall continental weatherability through this short term CO_2 consumption mechanism as well.

Dust promotes atmospheric CO_2 consumption by silicate weathering. Global continental weatherability has been elevated by dust transport to humid regions in multiple ways, but only atmospheric CO_2 consumption by silicate weathering can be estimated because the biogeochemical impact of dust and climate modulated dust carbonate weathering rate are difficult to assess quantitatively. In the context of dust silicate weathering, with an increase in MAP, the degree of silicate weathering alternation has increased, as shown by the decreasing Na_2O/Al_2O_3 ratio and the increasing long term atmospheric CO_2 consumption efficiency (a measure of the amount of CO_2 consumed by silicate weathering *per* kilogram rock) (Fig. S-7). We use the dust silicate weathering and the associated CO_2 consumption efficiency in regions with MAP <200 mm as a base value to evaluate the increases in dust deposition flux and the associated atmospheric CO_2 consumption in each climate zone with MAP >200 mm (Supplementary Information, Fig. 2). The additional long term atmospheric CO_2 consumption flux by silicate weathering yielded 0.431 ± 0.030 Tmol yr^{-1} and 0.503 ± 0.037 Tmol yr^{-1} for regions with MAP >400 mm and MAP >200 mm during the LGM period, respectively. Such fluxes are significant and represent 15–19 % of modern day long term global continental silicate weathering (Gaillardet *et al.*, 1999). On the other hand, the cooling by 4.4–6.8 °C from PI to LGM conditions used in our modelling would at least lower modern day silicate weathering by 23 to 35 %, depending on the type of lithology and parametric laws used (West, 2012; Li *et al.*, 2016). Our calculation shows that the increase in weatherability related to enhanced dust production and transport under the LGM is likely to be as important as the effect of global temperature decrease on atmospheric CO_2 consumption by silicate weathering, which may sustain less variable silicate weathering flux into the ocean at glacial-interglacial timescales (*e.g.*, von Blanckenburg *et al.*, 2015).

Implications

Our study suggests that a dustier world in glacial periods comes with higher land surface weatherability during the late Neogene cooling, where higher land surface weatherability caused by aeolian dust can have an enhanced ability to buffer the carbon cycle fluctuation. A dusty world may have appeared in the Neogene, because modern major global dust source areas, *e.g.*, North Africa and the broad Asian arid region, were formed during the Neogene (Guo *et al.*, 2002; Zhang *et al.*, 2014). Pre-Quaternary global dust deposition is difficult to constrain due to a paucity of robust boundary conditions (*e.g.*, vegetation) and palaeo-dust reconstructions. The global dust emission of the mid-Pliocene (3.3–3.0 Ma, a warm period prior to Quaternary glacial cycles) was only half or even less of that in the PI period (Shi *et al.*, 2011; Sagoo and Storelvmo, 2017), which may suggest less dust deposition in warming periods during the late Neogene on timescales of millions of years. This aeolian dust-driven high degree of weatherability in a cooling world may provide an independent explanation for the overall low levels of atmospheric CO_2 in the Neogene and similar cooling stages during the deep past, but it requires to be further examined by more robust palaeo-dust reconstruction and modelling.

Acknowledgements

This study was supported by the National Key Research and Development Program of China (2022YFF0800502), the Second Tibetan Plateau Scientific Expedition and Research (2019QZKK0707), and the National Natural Science Foundation of China (42171010, 42002129). AG was supported by ANR GI-NOAH (ANR-19-CE01-0014), and FL acknowledges support from projects ANID FONDECYT 1191223 and FONDAP 1522A0001. Yonggang Liu is thanked for dust modelling assistance. Two anonymous reviewers are thanked for their helpful comments.

Editor: Gavin Foster

Additional Information

Supplementary Information accompanies this letter at https://www.geochemicalperspectivesletters.org/article2322.

Cite this letter as: Yang, Y., Galy, A., Zhang, J., Lambert, F., Zhang, M., Zhang, F., Fang, X. (2023) Dust transport enhanced land surface weatherability in a cooling world. *Geochem. Persp. Let.* 26, 36–39. https://doi.org/10.7185/geochemlet.2322

References

Caves, J.K., Jost, A.B., Lau, K.V., Maher, K. (2016) Cenozoic carbon cycle imbalances and a variable weathering feedback. *Earth and Planetary Science Letters* 450, 152–163. https://doi.org/10.1016/j.epsl.2016.06.035

Caves Rugenstein, J.K., Ibarra, D.E., von Blanckenburg, F. (2019) Neogene cooling driven by land surface reactivity rather than increased weathering fluxes. *Nature* 571, 99–102. https://doi.org/10.1038/s41586-019-1332-y

Chadwick, O.A., Derry, L.A., Vitousek, P.M., Huebert, B.J., Hedin, L.O. (1999) Changing sources of nutrients during four million years of ecosystem development. *Nature* 397, 491–497. https://doi.org/10.1038/17276

Clift., P.D. (2006) Controls on the erosion of Cenozoic Asia and the flux of clastic sediment to the ocean. *Earth and Planetary Science Letters* 241, 571–580. https://doi.org/10.1016/j.epsl.2005.11.028

Francois, L.M., Walker, J.C.G. (1992) Modelling the Phanerozoic carbon cycle and climate: constraints from the $^{87}Sr/^{86}Sr$ isotopic ratio of seawater. *American Journal of Science* 292, 81–135. https://doi.org/10.2475/ajs.292.2.81

Gaillardet, J., Dupré, B., Louvat, P., Allègre, C.J. (1999) Global silicate weathering and CO_2 consumption rates deduced from the chemistry of large rivers. *Chemical Geology* 159, 3–30. https://doi.org/10.1016/S0009-2541(99)00031-5

Galy, A., France-Lanord, C. (1999) Weathering processes in the Ganges–Brahmaputra basin and the riverine alkalinity budget. *Chemical Geology* 159, 31–60. https://doi.org/10.1016/S0009-2541(99)00033-9

Goddéris, Y., Williams, J.Z., Schott, J., Pollard, D., Brantley, S.L. (2010) Time evolution of the mineralogical composition of Mississippi Valley loess over the last 10 kyr: Climate and geochemical modeling. *Geochimica et Cosmochimica Acta* 74, 6357–6374. https://doi.org/10.1016/j.gca.2010.08.023

Goddéris, Y., Brantley, S.L., François, L.M., Schott, J., Pollard, D., Déqué, M., Dury, M. (2013) Rates of consumption of atmospheric CO_2 through the weathering of loess during the next 100 yr of climate change. *Biogeosciences* 10, 135–148. https://doi.org/10.5194/bg-10-135-2013

Guo, Z.T., Ruddiman, W.F., Hao, Q.Z., Wu, H.B., Qiao, Y.S., Zhu, R.X., Peng, S.Z., Wei, J.J., Yuan, B.Y., Liu, T.S. (2002) Onset of Asian desertification by 22 Myr ago inferred from loess deposits in China. *Nature* 416, 159–163. https://doi.org/10.1038/416159a

Herman, F., Seward, D., Valla, P.G., Carter, A., Kohn, B., Willett, S.D., Ehlers, T.A. (2013) Worldwide acceleration of mountain erosion under a cooling Climate. *Nature* 504, 423–426. https://doi.org/10.1038/nature12877

Kump, L.R., Arthur, M.A. (1997) Global Chemical Erosion during the Cenozoic: Weatherability Balances the Budgets. In: Ruddiman, W.F. (Ed.) *Tectonic Uplift and Climate Change*. Springer, Boston, 399–426. https://doi.org/10.1007/978-1-4615-5935-1_18

Kurtz, A.C., Derry, L.A., Chadwick, O.A. (2001) Accretion of Asian dust to Hawaiian soils: isotopic, elemental, and mineral mass balances. *Geochimica et Cosmochimica Acta* 65, 1971–1983. https://doi.org/10.1016/S0016-7037(01)00575-0

Lenard, S.J.P., Lave, J., France-Lanord, C., Aumaitre, G., Bourlès, D.L., Keddadouche, K. (2020) Steady erosion rates in the Himalayas through late Cenozoic climatic changes. *Nature Geoscience* 13, 448–452. https://doi.org/10.1038/s41561-020-0585-2

Li, G., Hartmann, J., Derry, L.A., West, A.J., You, C.-F., Long, X., Zhan, T., Li, L., Li, G., Qiu, W., Li, T., Liu, L., Chen, Y., Ji, J., Zhao, L., Chen, J. (2016) Temperature dependence of basalt weathering. *Earth and Planetary Science Letters* 443, 59–69. https://doi.org/10.1016/j.epsl.2016.03.015

Métivier, F., Gaudemer, Y., Tapponnier, P., Klein, M. (1999) Mass accumulation rates in Asia during the Cenozoic. *Geophysical Journal International* 137, 280–318. https://doi.org/10.1046/j.1365-246X.1999.00802.x

Park, Y., Maffre, P., Goddéris, Y., Macdonald, F.A., Anttila, E.S.C., Swanson-Hysell, N.L. (2020) Emergence of the southeast Asian islands as a driver for Neogene cooling. *Proceedings of the National Academy of Sciences* 117, 25319–25326. https://doi.org/10.1073/pnas.2011033117

Rao, W., Han, G., Tan, H., Jin, K., Wang, S., Chen, T. (2017) Chemical and Sr isotopic characteristics of rainwater on the Alxa Desert Plateau, North China: Implication for air quality and ion sources. *Atmospheric Research* 193, 163–172. https://doi.org/10.1016/j.atmosres.2017.04.007

Raymo, M.E., Ruddiman, W.F., Froelich, P.N. (1988) Influence of late Cenozoic mountain building on ocean geochemical cycles. *Geology* 16, 649–653. https://doi.org/10.1130/0091-7613(1988)016<0649:IOLCMB>2.3.CO;2

Ridgwell, A.J. (2002) Dust in the Earth system: the biogeochemical linking of land, air and sea. *Philosophical Transactions of the Royal Society A: Mathematical, Physical and Engineering Sciences* 360, 2905–2924. https://doi.org/10.1098/rsta.2002.1096

Sagoo, N., Storelvmo, T. (2017) Testing the sensitivity of past climates to the indirect effects of dust. *Geophysical Research Letters* 44, 5807–5817. https://doi.org/10.1002/2017GL072584

Shi, Z., Liu, X., An, Z., Yi, B., Yang, P., Mahowald, N. (2011) Simulated variations of eolian dust from inner Asian deserts at the mid-Pliocene, last glacial maximum, and present day: contributions from the regional tectonic uplift and global climate change. *Climate Dynamics*, 37, 2289–2301. https://doi.org/10.1007/s00382-011-1078-1

Swap, R., Garstang, M., Greco, S., Talbot, R., Kållberg, P. (1992) Saharan dust in the Amazon Basin. *Tellus B: Chemical and Physical Meteorology* 44, 133–149. https://doi.org/10.3402/tellusb.v44i2.15434

von Blanckenburg, F., Bouchez, J., Ibarra, D.E., Maher, K. (2015) Stable runoff and weathering fluxes into the oceans over Quaternary climate cycles. *Nature Geoscience* 8, 538–542. https://doi.org/10.1038/ngeo2452

Walker, J.C.G., Hays, P.B., Kasting, J.F. (1981) A negative feedback mechanism for the long-term stabilization of Earth's surface temperature. *Journal of Geophysical Research: Oceans* 86, 9776–9782. https://doi.org/10.1029/JC086iC10p09776

West, A.J. (2012) Thickness of the chemical weathering zone and implications for erosional and climatic drivers of weathering and for carbon-cycle feedbacks. *Geology* 40, 811–814. https://doi.org/10.1130/G33041.1

Yang, Y., Galy, A., Fang, X., France-Lanord, C., Wan, S., Yang, R., Zhang, J., Zhang, R., Yang, S., Miao, Y., Liu, Y., Ye, C. (2021) East Asian monsoon intensification promoted weathering of the magnesium-rich southern China upper crust and its global significance. *Science China Earth Sciences* 64, 1155–1170. https://doi.org/10.1007/s11430-020-9781-3

Zhang, Z., Ramstein, G., Schuster, M., Li, C., Contoux, C., Yan, Q. (2014) Aridification of the Sahara desert caused by Tethys Sea shrinkage during the Late Miocene. *Nature* 513, 401–404. https://doi.org/10.1038/nature13705

Geochemical Perspectives Letters

Dust transport enhanced land surface weatherability in a cooling world

Y. Yang, A. Galy, J. Zhang, F. Lambert, M. Zhang, F. Zhang, X. Fang

Supplementary Information

The Supplementary Information includes:

- Methods
- Figures S-1 to S-7
- Supplementary Information References

Methods

Dust model performed in this study

In this study, the climate model Community Earth System Model version 1.2.2 (CESM1.2.2; Hurrell *et al.*, 2013) is used, which was developed and is maintained by the National Center for Atmospheric Research. CESM1.2.2 can simulate the present climate well (Knutti *et al.*, 2013) and has also been widely used in palaeoclimate research (*e.g.*, Liu *et al.*, 2020; Zhang *et al.*, 2021). In this model, the atmospheric component, Community Atmosphere Model version 5 (CAM5), is run at a horizontal resolution of ~1.9° (latitude) × 2.5° (longitude) with 30 levels in the vertical dimension, and each cell considers the emission, transport and deposition of dust (Ganopolski *et al.*, 2010). The land module, Community Land Model version 4.0 (CLM4.0), is run at the same horizontal resolution as CAM5.

Both palaeoclimate records and climate models suggest that the global mean surface temperature during the LGM was 4.4–6.8 °C lower than that in preindustrial times (Tierney *et al.*, 2020; Osman *et al.*, 2021) and that the land ice sheet was much greater during the LGM (Peltier *et al.*, 2015). These two points are considered in LGM-Exp. The orbital parameters and the levels of greenhouse gases (GHGs) during the LGM follow the Palaeoclimate Modelling Intercomparison Project phase 3 (PMIP3) protocol. The vegetation cover for the LGM-Exp corresponds to a modified PI-Exp vegetation cover according to the response of vegetation phenology to climate change based on the active CN biogeochemical cycle (Lawrence *et al.*, 2011).

In PI-Exp, the sea surface temperatures (SSTs) and sea ice fractions correspond to the default values of the CESM. LGM-Exp is run with the SSTs and sea ice fractions resulting from the equilibrium of a coupled run with the settings of Zhang *et al.* (2022). PI-Exp and LGM-Exp were run for 20 years, and only the data corresponding to the last 10 years are analysed and presented here.

On land, the annual mean precipitation from North Africa to inland Asia is less than 200 mm in PI-Exp, where the dust deposition fluxes are the greatest across the world (Fig. S-1a). This dust deposition pattern is also consistent with modern observations (Jickells *et al.*, 2005). As global cooling occurred during the LGM period, the land area with annual mean precipitation less than 200 mm expanded poleward in the Northern Hemisphere, and the global dust deposition fluxes increased obviously (Fig. S-1b). A drier and dustier world during the LGM is in accordance with previous simulations (*e.g.*, Lambert *et al.*, 2015, 2021) and geological reconstructions (*e.g.*, Lorius *et al.*, 1984; Maher *et al.*, 2010). We also modelled the near-surface winds in the two experiments (Figs. S-2, S-3), showing that the winds can transport dust out from arid regions (<200 mm and <400 mm MAP).

Collection of land dust deposition from other models

Our simulations produced just a single realisation of PI and LGM dust deposition fields. To estimate the uncertainty of the dust deposition fields, we also compiled paired PI and LGM dust deposition fluxes from four previously published studies (Takemura *et al*., 2009; Yukimoto *et al*., 2012; Albani *et al*., 2014; Lambert *et al*., 2015). Note that we chose a subset of available palaeoclimatic dust simulations. Because the observed modern global dust deposition is less than 3500 Tg yr^{-1} and there is a much larger LGM dust flux derived from palaeo-reconstructions (Maher *et al.*, 2010), those models with PI-derived global dust deposition >3500 Tg yr^{-1} or with a dust deposition ratio of LGM/PI < 2 are not included in our compilation.

Calculation of atmospheric CO_2 consumption by silicate weathering

To quantitatively assess the atmospheric CO_2 consumption by dust silicate weathering, we established a transformation equation from the degree of silicate Na depletion to atmospheric CO_2 consumption. The degree of Na depletion is a useful proxy for tracing silicate weathering intensity because plagioclase is the most common silicate mineral prone to weathering in the upper continental crust. Na depletion in silicates expressed by Na_2O/Al_2O_3 or τ_{Na} in soil or surface sediments shows a clear dependence on MAP at continental or global scales (Fig. S-5), regardless of lithology, suggesting that it is useful to trace the degree of dust silicate depletion in each MAP zone globally.

First, we establish a transformation equation from the Na_2O/Al_2O_3 silicate of surface soil to long term atmospheric CO_2 consumption *per* kilogram rock (hereafter atmospheric CO_2 consumption efficiency, mol kg^{-1}). Here, the CO_2 consumption efficiency is calculated by the chemical difference between soil and parent rock following France-Lanord and Derry (1997):

$$CO_2 \text{ consumption efficiency} = \Delta Ca + \Delta Mg + 0.10\ \Delta K + 0.15\ \Delta Na\ ,$$

where Δ shows the difference in base cations (Ca, Na, K, and Mg) between soil and parent rock. Note that the CO_2 consumption efficiency in this study reflects the atmospheric CO_2 consumption *per* kilogram rock on million-year timescales because only a fraction of the alkalinity is associated with alkalis (20 % for K^+ and 30 % for Na^+) (France-Lanord and Derry, 1997), thus providing a lower-limit estimate. Similar to Yang *et al*. (2021), we use loess and palaeosol samples in arid northern China and three average compositions of typical red soil datasets in humid southern China as well as the upper crust composition of central East China to yield a linear regression between Na_2O/Al_2O_3 and CO_2 consumption efficiency (Fig. S-6). These data were collected from a range of climatic settings and have an excellent linear distribution, suggesting a close link between the degree of Na depletion and the overall depletion of base cations in silicates.

Second, by using a recently reported dataset of surface soil Na_2O/Al_2O_3 ratios across China, we recalculated the soil Na_2O/Al_2O_3 ratio distribution in each MAP zone (Fig. S-7a). By using the transformation equation from Na_2O/Al_2O_3 to CO_2 consumption efficiency, we are able to estimate the CO_2 consumption efficiency in each MAP zone (Fig. S-7b). The increase in CO_2 consumption efficiency when dust is transported to less arid regions should correct CO_2 consumption efficiency in arid regions. Thus, the increase in CO_2 consumption efficiency in each less arid region is estimated to be the difference in CO_2 consumption efficiency between each region with MAP > 200 mm and the arid zone with MAP < 200 mm (Fig. 2b). Based on the increase in dust deposition fluxes in each MAP zone (Fig. 2a), the increase in CO_2 consumption flux by dust silicate weathering in each MAP zone (MAP > 200 mm) can be calculated (Fig. 2c).

Due to a lack of data, the dataset of surface soils in China is used to obtain a transformation equation for a global estimate, which inevitably yields bias. However, such a bias may be insignificant. First, the dataset includes 1996 surface soil composition data across variable lithology and climate settings (Guo *et al.*, 2022), thus reflecting a continental-scale Na_2O/Al_2O_3 distribution. Second, plagioclase is widely seen in granitic and basaltic rocks, which suggests that Na/Al can be widely used to trace silicate weathering in variable lithologies. Third, the similar mean composition of the upper continental crust between China and other commonly used estimates from different continents (Gao *et al*., 1998) suggests that data from the Chinese continent are suitable for conducting a global estimate. More importantly, what we try to estimate is indeed the difference in the silicate Na_2O/Al_2O_3 ratio between the less arid region with MAP > 200 mm and the arid region with MAP < 200 m, which should be less influenced by the absolute value of Na_2O/Al_2O_3 in different types of parent rocks. For example, Yang *et al*. (2021) evaluated the lithology impact, and they used different Na_2O/Al_2O_3 ratios of upper continental crust ranging from 0.20 to 0.25 as parent rocks to produce a linear regression line between Na_2O/Al_2O_3 and CO_2 consumption efficiency in surface soil. They found that the estimated difference in CO_2 consumption efficiency from Na_2O/Al_2O_3 ratios tends to be more consistent in different regressions, although the corresponding CO_2 consumption efficiency value in each regression exhibits slightly larger variabilities.

Supplementary Figures

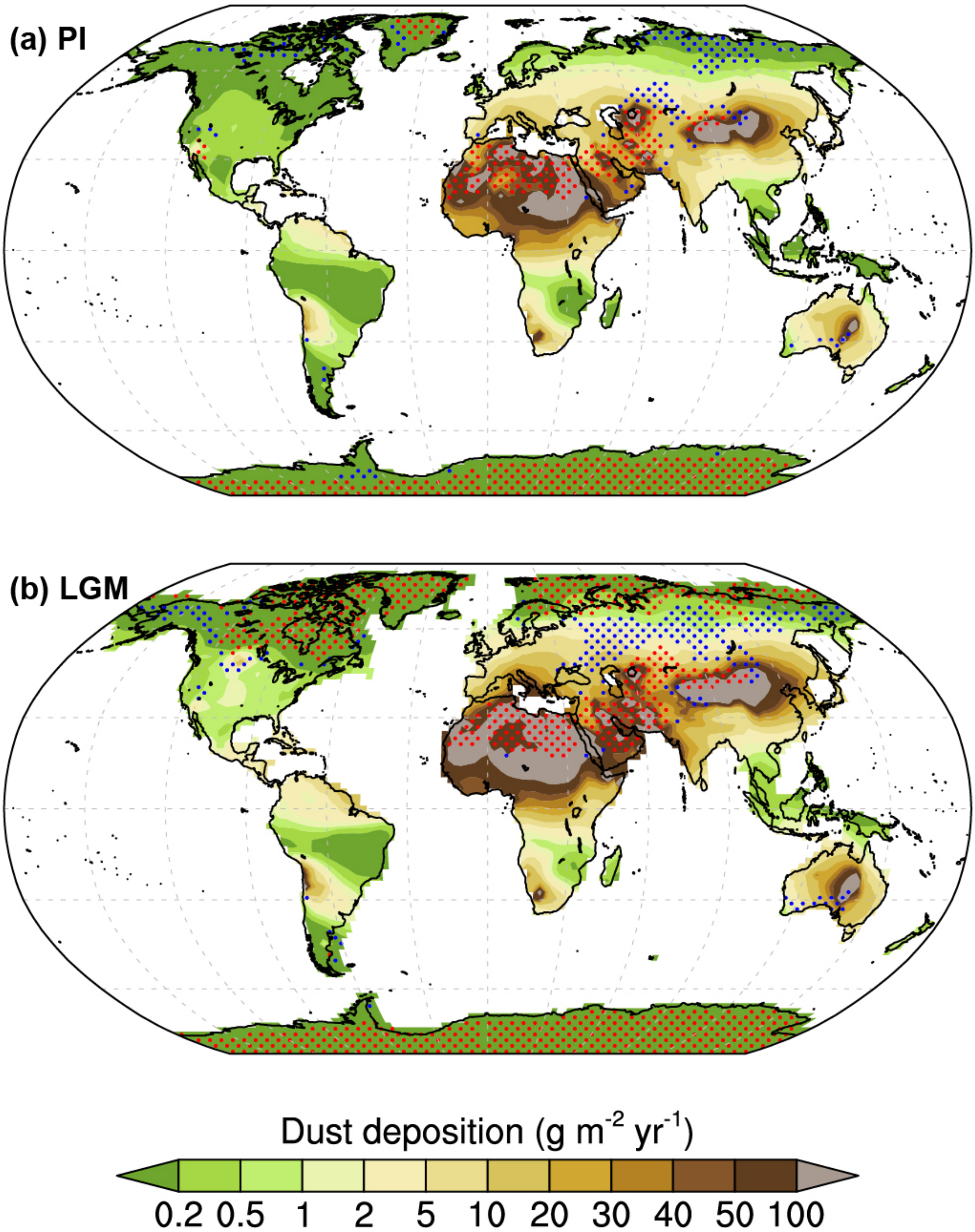

Figure S-1 Modelled land dust deposition (colour gradient, in g m^{-2} yr^{-1}) in experiments of **(a)** preindustrial (PI) and **(b)** Last Glacial Maximum (LGM) periods conducted from this study. Red and blue dots mark regions with mean annual precipitation (MAP) of <200 mm and 200–400 mm, respectively.

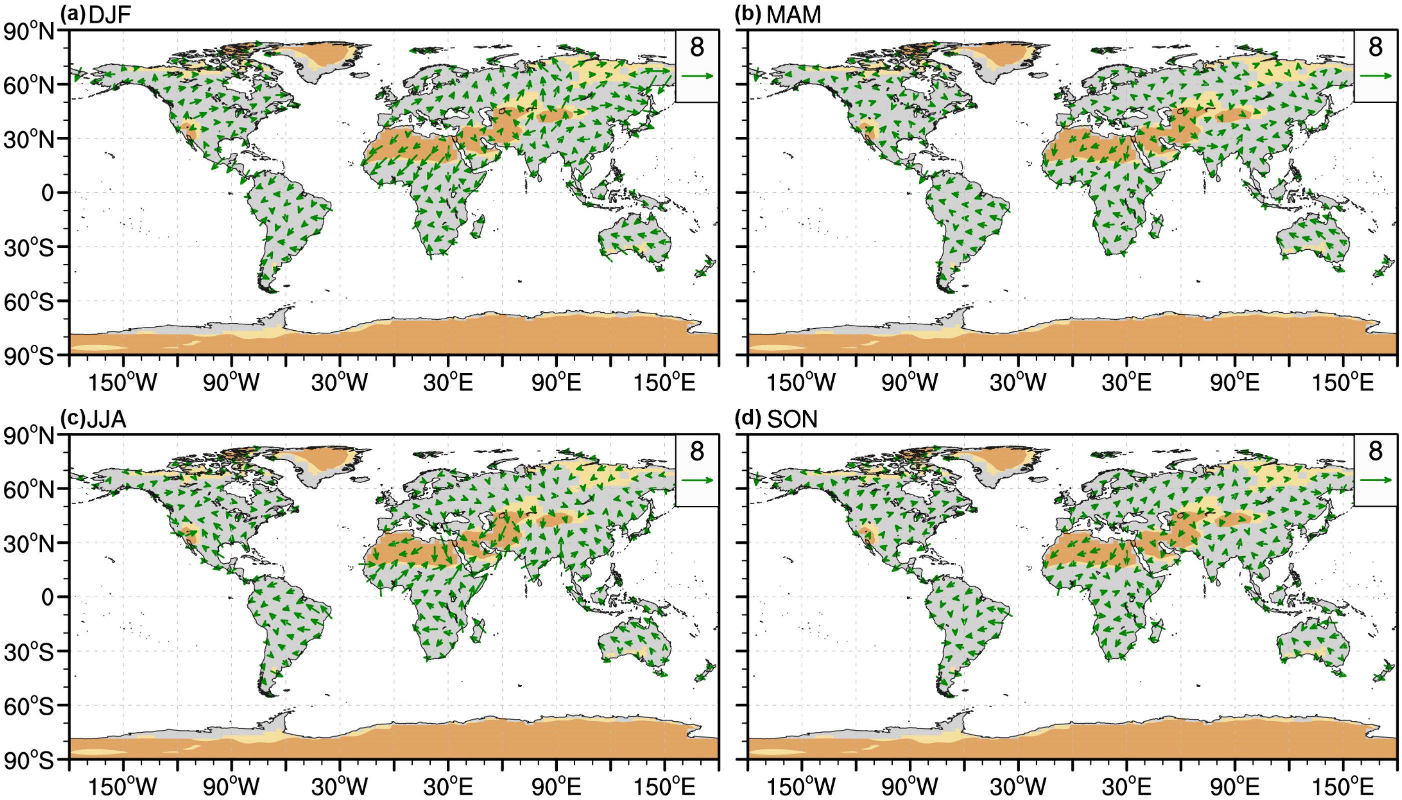

Figure S-2 Annual mean precipitation (shaded: orange, MAP < 200 mm; yellow, MAP = 200–400 mm) and four seasonal mean winds (vectors; units: m s^{-1}) near the surface of PI-Exp from this study. **(a)** DJF, **(b)** MAM, **(c)** JJA, **(d)** SON.

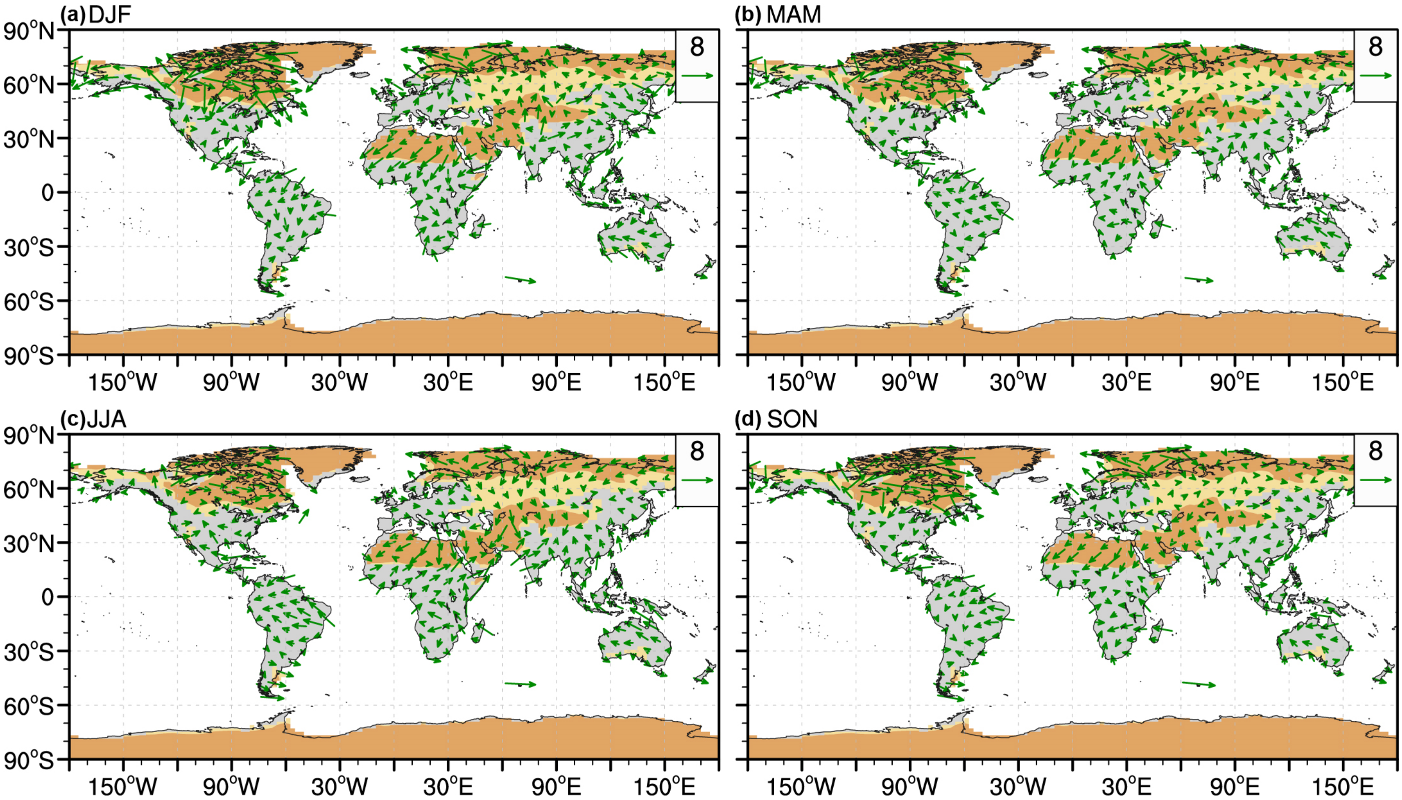

Figure S-3 Annual mean precipitation (shaded: orange, MAP < 200 mm; yellow, MAP = 200–400 mm) and four seasonal mean winds (vectors; units: m s^{-1}) near the surface of LGM-Exp from this study. **(a)** DJF, **(b)** MAM, **(c)** JJA, **(d)** SON.

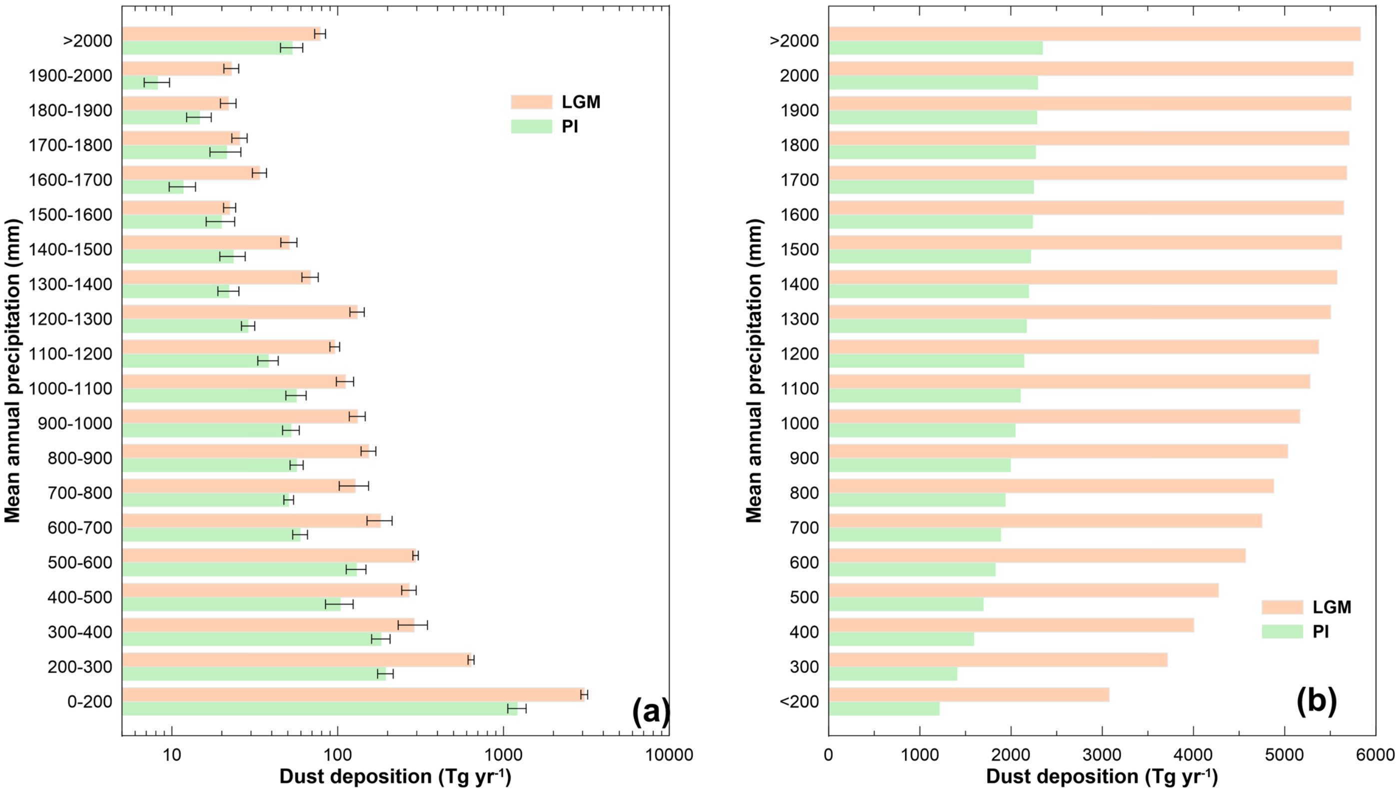

Figure S-4 Mean land dust deposition in experiments of preindustrial (PI) and Last Glacial Maximum (LGM) periods. **(a)** Mean land dust deposition in each MAP range; **(b)** accumulation of land dust deposition from low to high MAP. Error bars in **(a)** mark one standard error of the mean, and statistics are compiled from five dust deposition datasets (see Methods).

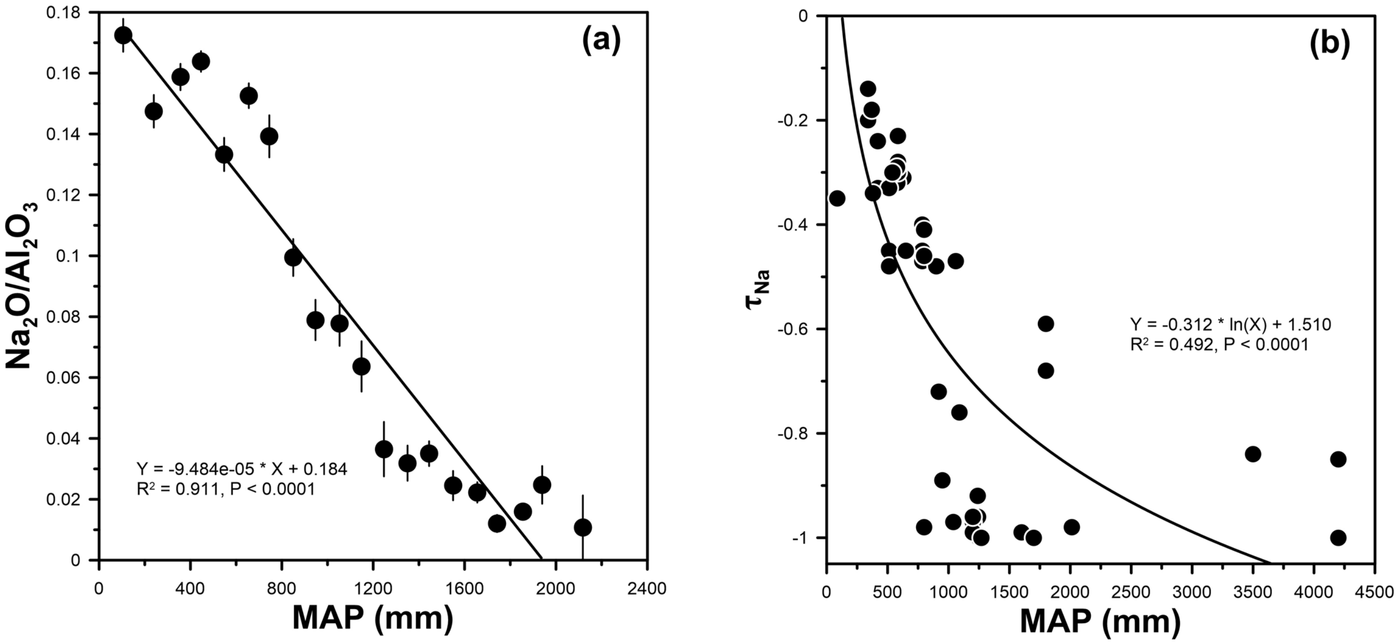

Figure S-5 Correlation of the degree of silicate Na depletion in surface soils with MAP. **(a)** Mean Na_2O/Al_2O_3 ratio of bulk surface soil across China in each MAP zone (data from Guo *et al*., 2022, MAP division follows Fig. 2). Error bars mark one standard error of the mean. **(b)** τ_{Na} in global soils with MAP (data from Brantley *et al*., 2023). τ_{Na} shows differences in the Na/Zr ratio between soil and parent rock, and a more negative τ_{Na} indicates a higher degree of Na depletion.

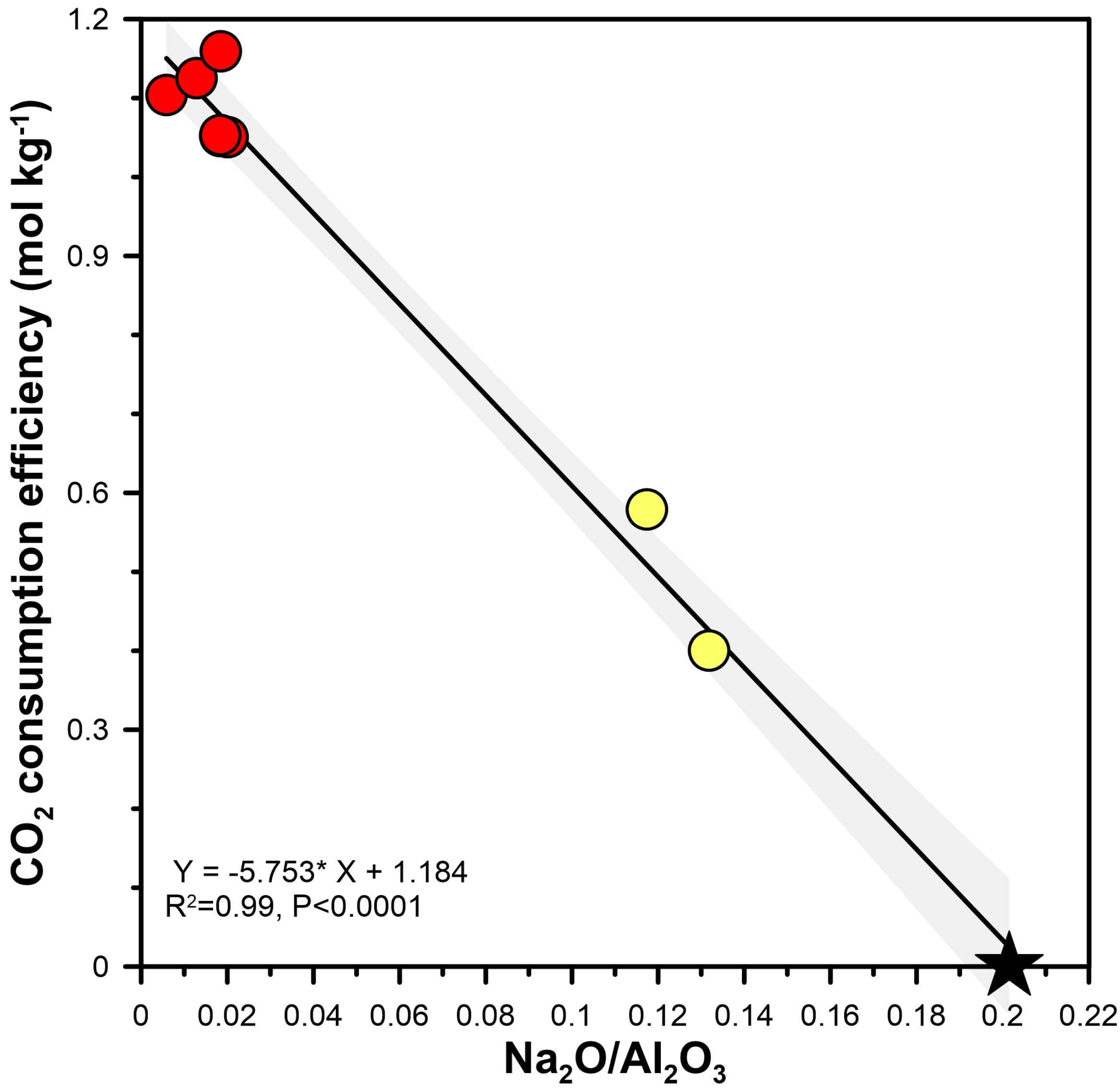

Figure S-6 Correlation between Na_2O/Al_2O_3 and long-term CO_2 consumption efficiency for loess and palaeosol samples (yellow dots) in northern China and three average compositions of typical red soil (red dots) datasets in southern China. The upper crust composition of East China (black pentagram; Gao *et al.*, 1998) is chosen as the parent rock. All data are from Yang *et al.* (2021), and the calculation of CO_2 consumption efficiency can be found in Methods. These data form an excellent fit line with 95 % confidence (shading area), which thus yields a transfer equation from silicate Na_2O/Al_2O_3 to long term CO_2 consumption efficiency in Figure S-7.

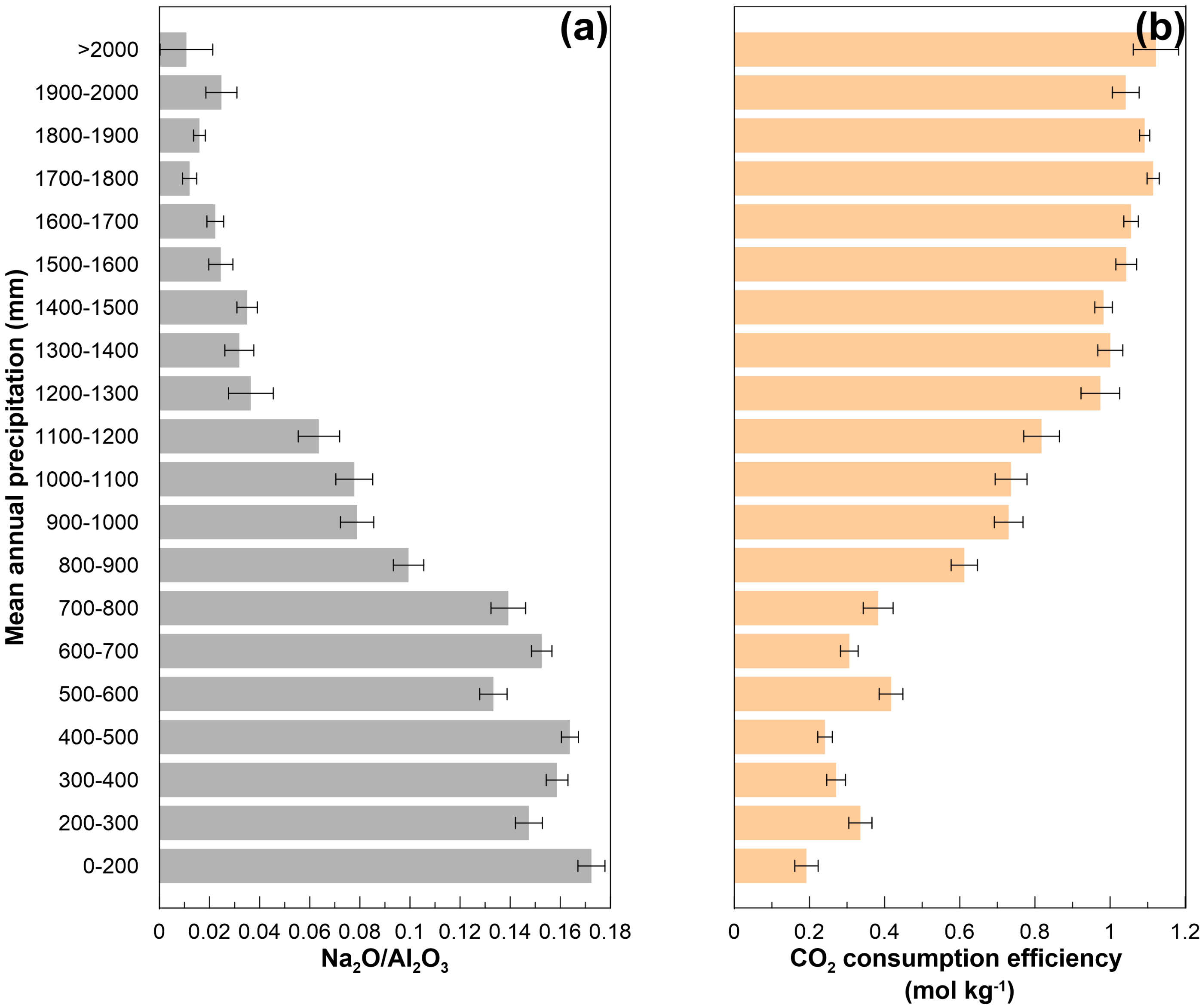

Figure S-7 **(a)** Averages of Na_2O/Al_2O_3 in bulk surface soil across China categorised by mean annual precipitation (data are from Guo *et al*., 2022) and **(b)** associated CO_2 consumption efficiency calculated by the equation in Figure S-6. Error bars mark one standard error of the mean.

Supplementary Information References

Albani, S., Mahowald, N.M., Perry, A.T., Scanza, R.A., Zender, C.S., Heavens, N.G., Maggi, V., Kok, J.F., Otto-Bliesner, B.L. (2014) Improved dust representation in the community atmosphere model. *Journal of Advances in Modeling Earth Systems* 6, 541–570. https://doi.org/10.1002/2013MS000279

Brantley, S., Shaughnessy, A., Lebedeva, M.I., Balashov, V.N. (2023) How temperature-dependent silicate weathering acts as Earth's geological thermostat. *Science* 379, 382–389. https://doi.org/10.1126/science.add2922

France-Lanord, C., Derry, L.A. (1997) Organic carbon burial forcing of the carbon cycle from Himalayan erosion. *Nature* 390, 65–67. https://doi.org/10.1038/36324

Ganopolski, A., Calov, R., Claussen, M. (2010) Simulation of the last glacial cycle with a coupled climate ice-sheet model of intermediate complexity. *Climate of the Past* 6, 229–244. https://doi.org/10.5194/cp-6-229-2010

Gao, S., Luo, T.-C., Zhang, B.-R., Zhang, H.-F., Han, Y.-W., Zhao, Z.-D., Hu, Y.-K. (1998) Chemical composition of the continental crust as revealed by studies in east China. *Geochimica et Cosmochimica Acta* 62, 1959–1975. https://doi.org/10.1016/S0016-7037(98)00121-5

Guo, L., Wu, J., Chen, Y., Xiong, S., Cui, J., Ding, Z. (2022) Modern silicate weathering regimes across China revealed by geochemical records from surface soils. *Journal of Geophysical Research: Earth Surface* 127, e2022JF006728. https://doi.org/10.1029/2022JF006728

Hurrell, J.W., Holland, M.M., Gent, P.R., Ghan, S., Kay, J.E., Kushner, P.J., Lamarque, J.F., Large, W.G., Lawrence, D., Lindsay, K., Lipscomb, W.H. (2013) The community earth system model: a framework for collaborative research. *Bulletin of the American Meteorological Society* 94, 1339–1360. https://doi.org/10.1175/BAMS-D-12-00121.1

Jickells, T.D., An, Z.S., Andersen, K.K., Baker, A.R., Bergametti, G., Brooks, N., Cao, J.J., Boyd, P.W., Duce, R.A., Hunter, K.A., Kawahata, H. (2005) Global iron connections between desert dust, ocean biogeochemistry, and climate. *Science* 308, 67–71. https://doi.org/10.1126/science.1105959

Knutti, R., Masson, D. Gettelman, A. (2013) Climate model genealogy: Generation CMIP5 and how we got there. *Geophysical Research Letters* 40, 1194–1199. https://doi.org/10.1002/grl.50256

Lambert, F., Tagliabue, A., Shaffer, G., Lamy, F., Winckler, G., Farias, L., Gallardo, L., De Pol-Holz, R. (2015) Dust fluxes and iron fertilization in Holocene and Last Glacial Maximum climates. *Geophysical Research Letters* 42, 6014–6023. https://doi.org/10.1002/2015GL064250

Lambert, F., Opazo, N., Ridgwell, A., Winckler, G., Lamy, F., Shaffer, G., Kohfeld, K., Ohgaito R., Albani, S., Abe-Ouchi, A. (2021) Regional patterns and temporal evolution of ocean iron fertilization and CO_2 drawdown during the last glacial termination. *Earth and Planetary Science Letters* 554, 116675. https://doi.org/10.1016/j.epsl.2020.116675

Lawrence, D.M., Oleson, K.W., Flanner, M.G., Thornton, P.E., Swenson, S.C., Lawrence, P.J., Zeng, X., Yang, Z.L., Levis, S., Sakaguchi, K., Bonan, G.B. (2011) Parameterization Improvements and Functional and Structural Advances in Version 4 of the Community Land Model. *Journal of Advances in Modeling Earth Systems* 3, M03001. https://doi.org/10.1029/2011MS00045

Liu, Y., Wu, Y., Lin, Z., Zhang, Y., Zhu, J., Yi, C. (2020) Simulated Impact of the Tibetan Glacier Expansion on the Eurasian Climate and Glacial Surface Mass Balance during the Last Glacial Maximum. *Journal of Climate* 33, 6491–6509. https://doi.org/10.1175/JCLI-D-19-0763.1

Lorius, C., Raynaud, D., Petit, J., Jouzel, J., Merlivat, L. (1984) Late-Glacial Maximum-Holocene Atmospheric and Ice-Thickness Changes from Antarctic Ice-Core Studies. *Annals of Glaciology* 5, 88–94. https://doi.org/10.3189/1984AoG5-1-88-94

Maher, B.A., Prospero, J.M., Mackie, D., Gaiero, D., Hesse, P.P., Balkanski, Y. (2010) Global connections between aeolian dust, climate and ocean biogeochemistry at the present day and at the last glacial maximum. *Earth-Science Reviews* 99, 61–97. https://doi.org/10.1016/j.earscirev.2009.12.001

Osman, M.B., Tierney, J.E., Zhu, J., Tardif, R., Hakim, G.J., King, J., Poulsen, C.J. (2021) Globally resolved surface temperatures since the Last Glacial Maximum. *Nature* 599, 239–244. https://doi.org/10.1038/s41586-021-03984-4

Peltier, W.R., Argus, D.F., Drummond, R. (2015) Space geodesy constrains ice age terminal deglaciation: The global ICE-6G_C (VM5a) model. *Journal of Geophysical Research: Solid Earth* 120, 450–487. https://doi.org/10.1002/2014JB011176

Takemura, T., Egashira, M., Matsuzawa, K., Ichijo, H., O'ishi, R., Abe-Ouchi, A. (2009) A simulation of the global distribution and radiative forcing of soil dust aerosols at the last glacial maximum. *Atmospheric Chemistry and Physics* 9, 3061–3073. https://doi.org/10.5194/acp-9-3061-2009.

Tierney, J.E., Zhu, J., King, J., Malevich, S.B., Hakim, G.J., Poulsen, C.J. (2020) Glacial cooling and climate sensitivity revisited. *Nature* 584, 569–573. https://doi.org/10.1038/s41586-020-2617-x

Yang, Y., Ye, C., Galy, A., Fang, X., Xue, Y., Liu, Y., Yang, R., Zhang, R., Han, W., Zhang, W., Ruan, X. (2021) Monsoon-enhanced silicate weathering as a new atmospheric CO_2 consumption mechanism contributing to fast Late Miocene global cooling. *Paleoceanography and Paleoclimatology* 36, e2020PA004008. https://doi.org/10.1029/2020PA004008

Yukimoto, S., Adachi, Y., Hosaka, M., Sakami, T., Yoshimura, H., Hirabara, M., Tanaka, T.Y., Shindo, E., Tsujino, H., Deushi, M., Mizuta, R., Yabu, S., Obata, A., Nakano, H., Koshiro, T., Ose, T., Kitoh, A. (2012) A new global climate model of the meteorological research institute: MRI-CGCM3. *Journal of the Meteorological Society of Japan* 90A, 23–64. https://doi.org/10.2151/jmsj.2012-A02.

Zhang, J., Liu, Y., Flögel, S., Zhang, T., Wang, C., Fang, X. (2021) Altitude of the East Asian Coastal Mountains and Their Influence on Asian Climate During Early Late Cretaceous. *Journal of Geophysical Research: Atmospheres* 126, e2020JD034413. https://doi.org/10.1029/2020JD034413

Zhang, M., Liu, Y., Zhu, J., Wang, Z., Liu, Z. (2022) Impact of dust on climate and AMOC during the Last Glacial Maximum Simulated by CESM1.2. *Geophysical Research Letters* 49, e2021GL096672. https://doi.org/10.1029/2021GL096672